GEOPHYSICS, VOL. 78, NO. 6 (NOVEMBER-DECEMBER 2013); P. P19–P27, 21 FIGS.
10.1190/GEO2013-0142.1

Downloaded 10/10/13 to 129.241.27.34. Redistribution subject to SEG license or copyright; see Terms of Use at http://library.seg.org/

# Repeatability issues of high-frequency signals emitted by air-gun arrays

Martin Landrø[1], Lasse Amundsen[2], and Jan Langhammer[3]

## ABSTRACT

Recent field measurements of the acoustic signals generated by marine seismic air-gun arrays showed that the amount of high-frequency signals (above 10 kHz) increased with the size and total volume of the gun array. We found that for frequencies between 10 and 20 kHz, a strong signal is observed 7–14 ms after the main peak of the source signal. We believe that this signal was generated by ghost cavitation. We observed that this signal was significantly stronger than the high-frequency signal generated at the same time as the peak signal occurs within the bandwidth between 10 and 20 kHz. We found that this high-frequency signal was fairly repeatable from one shot to another. By "fairly," we mean that individual high-frequency events were not repeatable; however, the envelope energy of this cascade of events was repeatable from one shot to another. The typical feature of the envelope of the high-frequency signal was that it lasted for approximately 6–7 ms and showed a monotonic increase in amplitude for the first 5–6 ms, followed by a sudden drop. The sea surface reflection coefficient for these high-frequency events seemed to decrease in magnitude as the frequency increased.

## INTRODUCTION

In this work, we study source signatures of a marine air-gun array recorded using a bandwidth of 0–62.5 kHz. The data were recorded by a hydrophone vertically located below the source at the seabed. Traditionally, the major interest for air-gun performance has been to model and measure the emitted acoustic signals within the seismic bandwidth (0–250 Hz). Ziolkowski (1970) presents a comprehensive theory for air-gun modeling. Landrø et al. (1993) present a method for water-gun modeling. It is well known that the water gun emits a very high-frequency signal due to the collapse of the water vapor cavity. It is interesting to note that Rayleigh (1917) derives a nonlinear differential equation describing the collapse of a cavity in water. In recent years, interest in the high-frequency signals produced by air-gun arrays has increased. Some recent studies (Goold and Fish, 1998; Breitzke et al., 2008; Amundsen and Landrø, 2010, 2011a, 2011b; Landrø et al., 2011) discuss and present hearing curves of marine mammals. Dolphins and white whales have excellent hearing capacity for frequencies between 10 and 100 kHz.

Southall et al. (2007) present a review on marine mammal hearing and suggest criteria for when various behavioral effects might occur. Laws (2010) uses the work of Southall et al. (2007) to estimate the extent of hearing damage zones around a seismic source. Groenaas et al. (2011) present a new system for detection of whales during seismic acquisition. In the proposed system, high-frequency hydrophones are used to detect the position of whales in the vicinity of the seismic vessel. The purpose of such a system is to stop seismic shooting if it is decided that it will influence the whale behavior significantly. Recently, Bolt Technology Corporation and WesternGeco have begun a joint effort to develop a new air gun. The objective for this new gun is to develop a bandwidth-controlled source designed to reduce the potential impact of seismic signals on marine life.

The work on defining criteria for acceptable noise thresholds is, as stated by Southall et al. (2007), not finalized, and it is therefore hard to judge whether the frequencies analyzed in this paper (between 10 and 60 kHz) will be of importance in the future. However, we think it is essential to understand various mechanisms that might make a significant amount of noise above 10 kHz. There are several factors related to the design and operation of individual air guns that we know generate high-frequency noise, such as the solenoid, the movement of the shuttle inside the gun, vibrations caused by jumping of the guns, and so on. In a recent paper on the same topic, Landrø et al. (2011) propose that cavities may be formed by the ghost signal from neighboring air guns. In this paper, we use the same data set, but we focus on how repeatable these signals are.

Manuscript received by the Editor 5 April 2013; revised manuscript received 7 June 2013; published online 7 October 2013.
[1]NTNU, Trondheim, Norway. E-mail: martin.landro@ntnu.no.
[2]NTNU and STATOIL Research Centre, Trondheim, Norway. E-mail: lam@statoil.com.
[3]Formerly OPTOPLAN, Trondheim, Norway; presently TGS, Asker, Norway. E-mail: jan.langhammer@tgs.com.
© 2013 Society of Exploration Geophysicists. All rights reserved.

Downloaded 10/10/13 to 129.241.27.34. Redistribution subject to SEG license or copyright; see Terms of Use at http://library.seg.org/

## THE FIELD EXPERIMENT

The field test was performed in the Black Sea offshore Turkey in December 2008. The shooting vessel was the M/V *Malene Østervold*, and several configurations of the source array were tested. The weather conditions were good (calm seas) during the experiment. The high-frequency data were recorded by an electrical hydrophone located at a fixed position at the sea bottom, using a sampling rate of 0.008 ms, which gives a Nyquist frequency of 62.5 kHz. We have no knowledge or measurements of water currents at the seabed and no knowledge of salinity variations. For each line, approximately 40 shots were taken as the ship was sailing on a straight line crossing over the sea bottom hydrophone (Figure 1). The water depth in the area varied between 50 and 60 m. In this paper, we analyze data from the line where the full array (2730 cubic inches) was used. The distance between the gun strings was 6 m. The array configuration is shown in Figure 2, and the source depth was 5 m for all shots in this line. We have no information about any firing time delays between various guns of the array. The precise position of the sea-bottom hydrophone relative to the source array is not known. However, from typical moveout curves, it is possible to find shots that are close to being straight above the hydrophone. For the present analysis, this lack of precise information does not create significant problems.

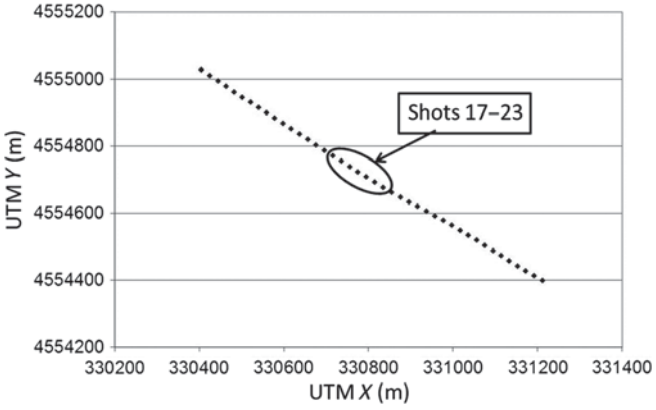
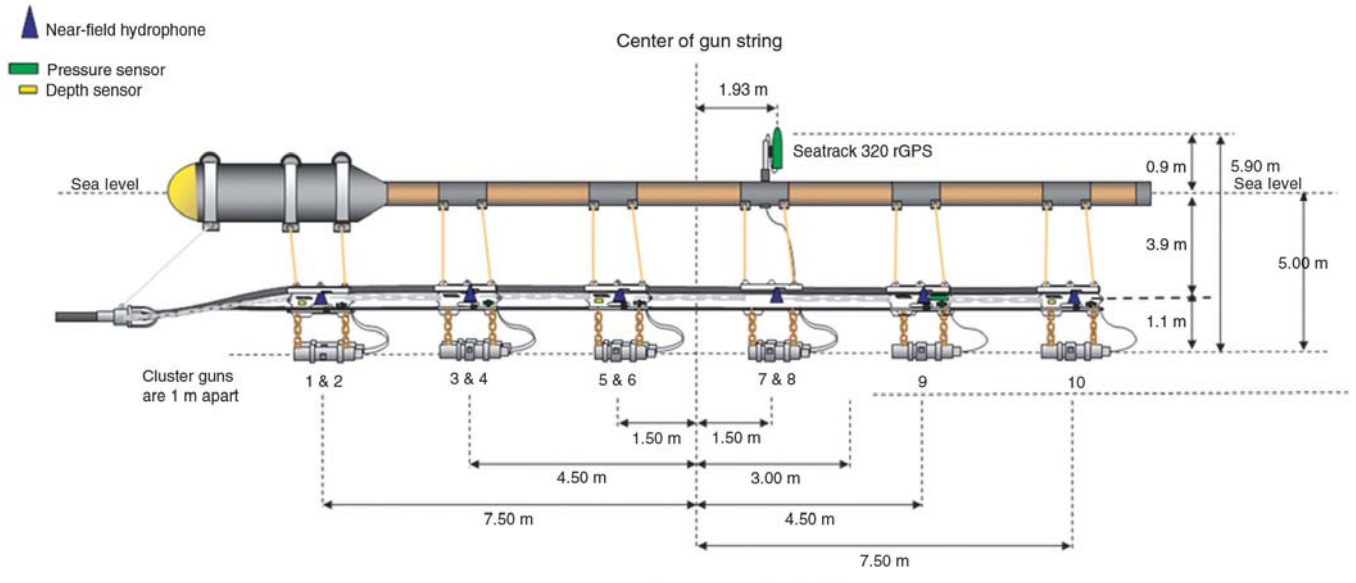



Figure 1. Universal transverse mercator coordinate system positions for the 42 shots. The exact position of the sea bottom hydrophone is not known and is therefore not shown. The distance between each shot is approximately 25 m.

## HOW REPEATABLE IS THE HIGH-FREQUENCY SIGNAL?

As Landrø et al. (2011) discuss, there is a characteristic high-frequency signal (between 10 and 50 kHz) associated with air-gun arrays that appears approximately 7–14 ms after the main peak. We suggest that the high-frequency signal (frequencies above 10 kHz) is caused by ghost cavitation, which is cavity formation located between the gun array substrings where the negative ghost signals results in pressures close to zero. Figure 3 shows 7 shots (17–23) where shot 20 is assumed to be relatively straight above




Gun volumes (cubic in.)

| | | | | | | |
|---|---|---|---|---|---|---|
| Array 1 | 250 | 70 | 150 | 100 | 100 | 70 |
| | 250 | 70 | 150 | 100 | | |
| Array 2 | 100 | 100 | 300 | 300 | 150 | 100 |
| | 100 | 100 | 300 | 300 | | |
| Array 3 | 250 | 70 | 150 | 100 | 100 | 70 |
| | 250 | 70 | 150 | 100 | | |

Figure 2. Array configuration: three strings separated by 6 m and deployed at 5 m depth. The gun volumes are listed in the table. The array consists of 12 two-gun clusters and 6 single guns.

Downloaded 10/10/13 to 129.241.27.34. Redistribution subject to SEG license or copyright; see Terms of Use at http://library.seg.org/

the hydrophone sensor. From these high-frequency measurements, we observe a varying delay time between individual guns in the array, creating slightly different shapes of the main peak signal. For seismic acquisition, this variation does not matter because these differences disappear when a typical seismic band-pass filter is applied, as shown in Figure 4.

However, when a high-frequency band-pass filter is applied to this data set, the main peak signal disappears and the maximum high-frequency signal occurs approximately 7–14 ms delayed compared to the main peak, as shown in Figure 5. There are some high-frequency signals at the same time as the main peak; however, these signals are significantly weaker compared to the signals appearing 7–14 ms later. It is hard to judge how repeatable the high-frequency signal is from one shot to another. Therefore, we used the absolute value of all samples and then applied a mean smoother (operator length of 1 ms) to the data, as shown in Figure 6. Here, we clearly see that the high-frequency signal is fairly repeatable: It has a relatively monotonic increase in amplitude until a maximum is reached, followed by a sudden decrease. On a more detailed level, we observe that these envelope traces are not perfectly repeated; there are details that vary between various shots. To ease this comparison further, we have aligned the signals (horizon flattening) in Figure 7.

It is interesting to observe that there is a similarity between the peak signals for shots 20 and 21 and the envelope of the high-frequency signals (Figure 8). For shot 20, we observe a local minimum at approximately 44 ms, and the same local minimum is observed for the envelope trace (to the right in Figure 8). For shot 21, there is no such local minimum for the unfiltered signal (left) and for the envelope signal (right). The crosscorrelation between the two traces is shown to the right in Figure 8. The correlation function is varying at the same rate as the traces, indicating that there is low repeatability for frequencies above 10 kHz.

An attempt to explain the observations made so far could be as follows: We assume that numerous small cavities are formed in the area between the air-gun strings, caused by the ghost signal from the free surface. These cavities collapse within a short time according to the formula Rayleigh (1917) derives,

$$T = 0.915R\sqrt{\frac{\rho}{p_h}}. \qquad (1)$$

Here, $T$ is the collapse time for the cavity, $R$ is the initial cavity radius, $\rho$ is the density of water, and $p_h$ is the hydrostatic pressure. If several cavities of various sizes collapse, their collapse time will also vary, and the biggest cavities will collapse at later times (equation 1). This might explain the typical monotonic increase in the envelope curves followed by a sudden decrease as displayed in Figure 7. However, we also observe significant shot-to-shot variations in Figure 7. These variations might be caused by variations in the state of the sea surface: If the reflection coefficient of the sea surface is varying from one shot to another, the amount of ghost cavities might be reduced, hence leading to a lower envelope signal. Another possible source for these variations might be swells causing variation

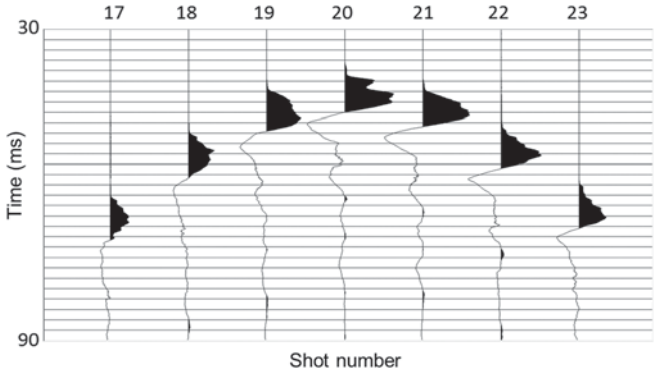



Figure 3. Seven traces corresponding to the shots closest to the sea-bottom high-frequency hydrophone. Trace 20 is closest to the hydrophone. We notice some variation in the primary peak, probably caused by slightly different firing time delays for individual guns. Notice the high-frequency noise occurring approximately 10 ms after the main peak. There are 2 m between each time line.

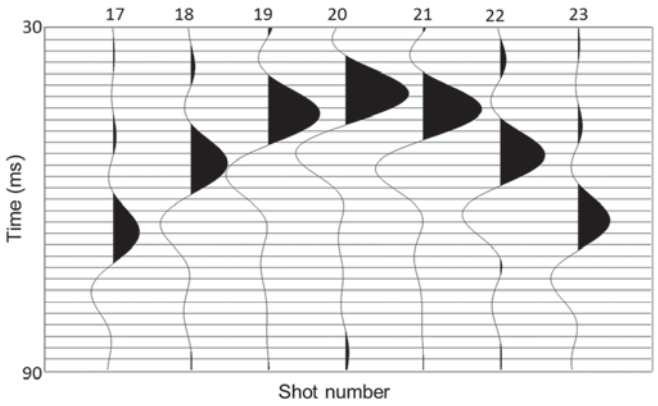



Figure 4. Bandpass filtered (0–10–60–80 Hz, Ormsby filter) version of shot records 17–23. No visible signs of individual guns are observed.

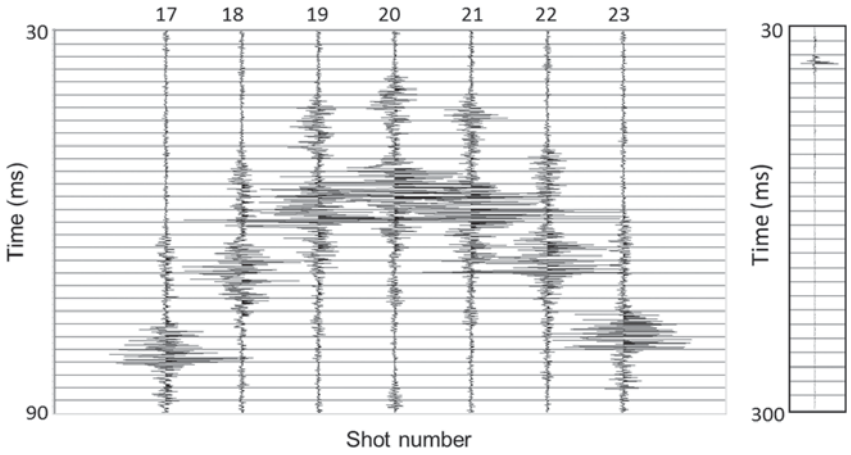



Figure 5. Same traces as Figure 3, after application of a 10–20 kHz band-pass filter. The high-frequency noise is now apparent. The trace to the right is included to show that there are no high-frequency signals occurring at later times (the record length is 300 ms).

Downloaded 10/10/13 to 129.241.27.34. Redistribution subject to SEG license or copyright; see Terms of Use at http://library.seg.org/

in gun depths from shot to shot. However, none of the proposed causes are very likely, because the weather conditions during the test were very good (calm seas). It is therefore most likely that these variations are caused by the geometry of the acquisition. Shot 17 is further away from the seabed hydrophone, resulting in weaker amplitudes and a different directivity pattern if we assume that the ghost cavitation signal is formed by several hundred cavities.

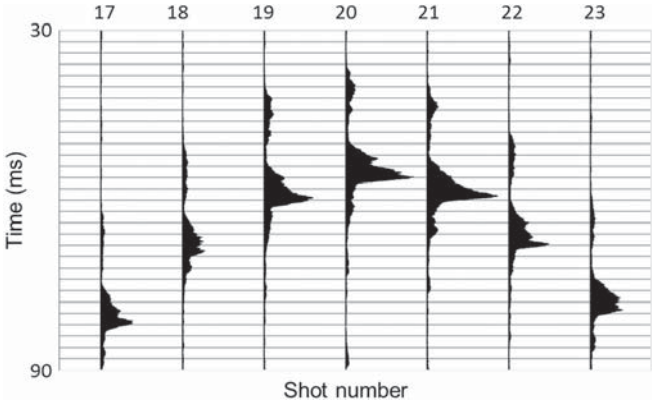



Figure 6. Same traces as Figure 4 after taking the absolute value of each sample and then applying a mean smoother with a window length of 1 ms.

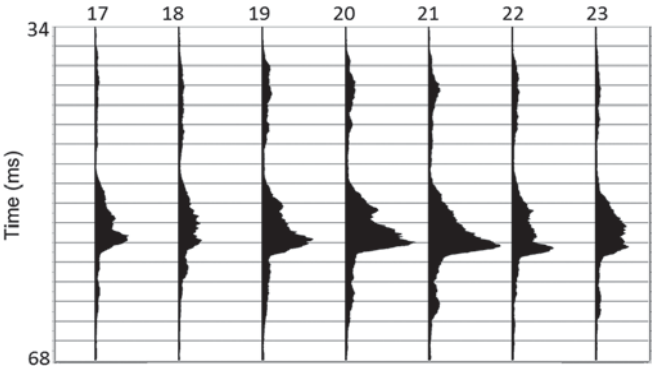



Figure 7. The same traces as in Figure 5, after horizon flattening. Notice the strong similarity between the traces: a close-to-monotonic increase followed by a steep decline in high-frequency signal strength.

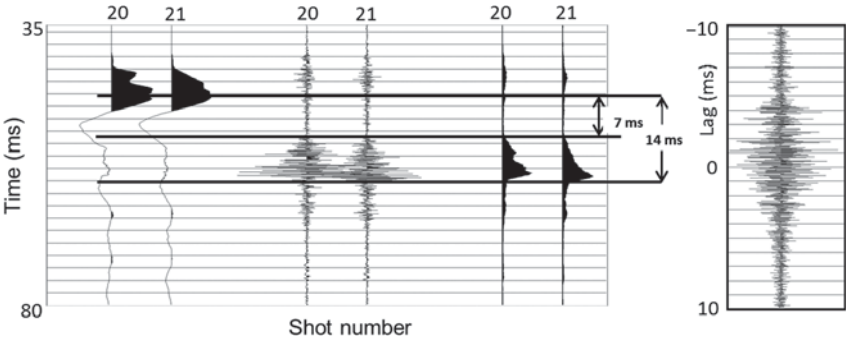



Figure 8. Detailed comparison of traces 20 and 21: Left, unfiltered; middle, after 10–20-kHz filtering; right, absolute value + mean smoother. A static shift has been applied to trace 21 to align them and ease the comparison. Time delays between the peak primary signal and the ghost cavity signals range between 7 and 14 ms. Far right, the crosscorrelation function between the two traces.

## THE TIME DELAY BETWEEN THE PEAK SIGNAL AND THE CAVITY SIGNAL

Our hypothesis for ghost cavity creation is sketched in Figure 9, where we assume that a cavity is created at a depth $z_1$ below the sea surface, and that two source subarrays (separated by a distance $2a$) are fired at a depth $z$. The traveltime for the direct arrival to the location of the birth of the cavity is given as

$$t_c = \frac{1}{c}\sqrt{(z+z_1)^2 + a^2}, \tag{2}$$

where $c$ is the P-wave velocity in water. The total traveltime needed to create the cavity, collapse it, and propagate the cavity signal to the seabed hydrophone is therefore

$$t_c = \frac{1}{c}\sqrt{(z+z_1)^2 + a^2} + 0.915R\sqrt{\frac{\rho}{p_0 + \rho g z_1}} + \frac{D - z_1}{c}, \tag{3}$$

where $p_0$ is the pressure at the sea surface and $D$ is the water depth. The corresponding traveltime for the direct arrival from the source to the hydrophone is

$$t_D = \frac{1}{c}\sqrt{(D-z)^2 + a^2}, \tag{4}$$

which means that the traveltime delay between the peak signal and the cavity signal ($\Delta t$) is given as

$$\Delta t = \frac{1}{c}\sqrt{(z+z_1)^2 + a^2} - \frac{1}{c}\sqrt{(D-z)^2 + a^2} + 0.915R\sqrt{\frac{\rho}{p_0 + \rho g z_1}} + \frac{D - z_1}{c}. \tag{5}$$

Figure 10 shows modeled time delay curves assuming an initial cavity radius of 1 mm (solid line) and 8 cm (dashed line), respectively. We notice that these numbers fit nicely with the observed time delays that range between 7 and 14 ms (Figure 8).

## COMPARISON WITH WATER-GUN SIGNATURES

Because we assume that the ghost cavitation noise is created by collapse of smaller cavities, it might be interesting to compare with water-gun signatures. We know that the main signal of a water gun is created by collapse of a water vapor cavity (Landrø et al., 1993). Unfortunately, we have only near-field measurements of two different water guns available for comparison. Still, we think it is interesting to compare the high-frequency noise from the air-gun array (that

Downloaded 10/10/13 to 129.241.27.34. Redistribution subject to SEG license or copyright; see Terms of Use at http://library.seg.org/

we interpret as cavitation noise) with measured water-gun signatures.

Figure 11 shows unfiltered versions of the far-field signatures recorded at the seabed approximately 60 m below the source array. We observe that for the big (2730 cubic inches) array (black solid line), the ghost signal occurs at 0.074 s. If we assume that cavities are formed in the region midway between the strings and at the same time as the ghost signal, it is possible to estimate the collapse time for individual cavities directly from the source signatures. A magnified version of the source signatures is shown in Figure 12, and we interpret two clear spikes (marked by arrows in the figure) as cavity collapses. We find that these two cavities collapse at 0.0783 and 0.0813 s and that the corresponding amplitude levels are 1.0 and 2.3 bar-m, respectively. If we assume that the cavities start to collapse when the ghost signal has a minimum, we find collapse times of 4.3 and 7.3 ms, and the corresponding initial radii of 5.7 and 9.7 cm, respectively, according to equation 1. These numbers maybe are not very realistic because, for instance, 100 cavities with a radius of 10 cm would occupy a volume of 420 liters. A comparison with near-field recordings from water guns might give us some further insight.

Figure 13 shows a near-field source signature of a S15 water gun. More details on water guns can be found in Landrø et al. (1993). This gun has four ports, which means that four cavities are formed at a certain distance from each port. However, in the near-field signature, it is not possible to see individual signals corresponding to each cavity. This indicates that the four cavities collapse at the same time. If we assume that the cavity starts to collapse at the minimum pressure level (at 0.02 s in Figure 13), we estimate a collapse time of 3 ms for the S15 water gun. This corresponds to an initial cavity radius of 4.3 cm, which is not too far from the initial radius (5.7 cm) estimated for the first cavity in Figure 12. The signature in Figure 13 has been acquired using a 800 Hz high-cut filter, and we observe that the maximum amplitude is approximately 0.8 bar-m, corresponding to 0.2 bar-m per cavity. The cavity signals marked by arrows in Figure 12 has a width of 0.1 ms, which means that they are not visible after applying a 800-Hz high-cut filter. In other words, a cavity with an initial radius of 4.3 cm will create a collapse signal that has a width of at least 1–2 ms. This is not observed for the data displayed in Figure 12. A similar near-field signature of a large water gun (with an air chamber volume of 400 cubic inches) is shown in Figure 14. For this case, we estimate a collapse time of 14 ms and a corresponding initial cavity radius of 0.2 m. The collapse signal is very strong in this case (11 bar-m). Based on this comparison, it is reasonable to assume that if the high-frequency signals observed in Figure 12 are caused by cavities collapsing, the collapse times and the sizes must be significantly smaller than those observed for water guns. Furthermore, it is fair to assume that the number of cavities is high, probably at least of the order of hundreds.

## THE GHOST CAVITATION MECHANISM

Plesset and Ellis (1955) demonstrate that it is possible to create cavities by acoustic stimulation. From their photos, it is evident that a cloud of small cavities is generated acoustically. Harrison (1952) uses a venturi nozzle to generate cavities and proves experimentally (using high-speed photographs) that Rayleigh's equation (equation 1 in this paper) is correct. If we assume that a similar mechanism occurs for the ghost cavitation that Landrø et al. (2011) suggest, it is

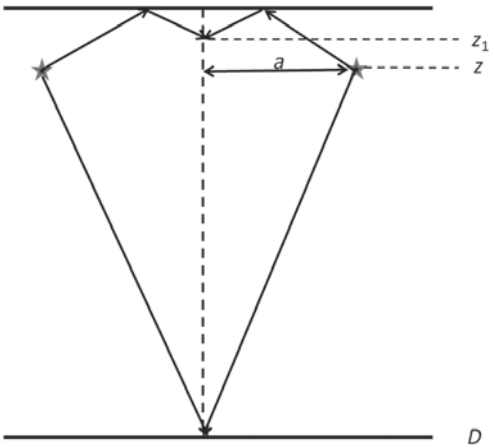



Figure 9. Sketch showing travel paths assuming that a cavity is formed midway between two source subarrays separated by a distance $2a$. The gun depth is $z$ and the depth where the cavity is formed is $z_1$. The water depth is $D$.

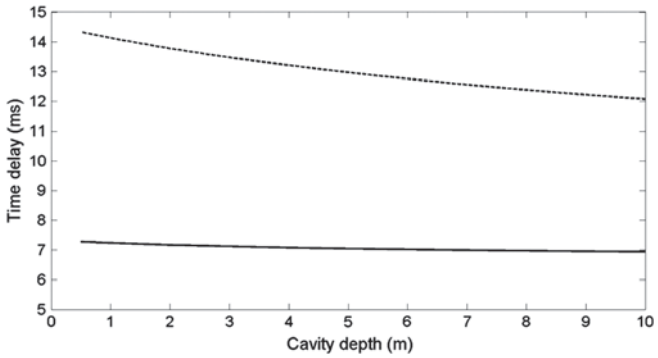



Figure 10. Modeled time delay between the direct arrival and the ghost signal as a function of cavity creation depth. The two subarrays are separated by 6 m. Solid line, cavity radius of 1 mm; dashed line, cavity radius of 8 cm. The source depth is 5 m, and the water depth is 60 m. Observed time delays from experimental data are between 7 and 14 ms (Figure 8).

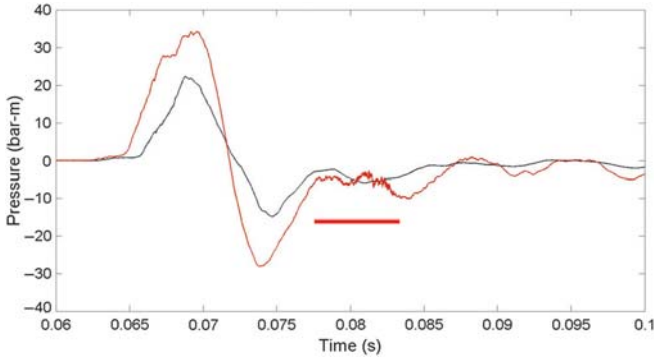



Figure 11. Source signatures from a single-string array (black solid line) and a multistring array (red solid line). The strongest ghost signal occurs at approximately 0.074 s for the multistring array. The high-frequency signal can be observed between 0.078 and 0.084 s. Figure reprinted from Landrø et al. (2011).

Downloaded 10/10/13 to 129.241.27.34. Redistribution subject to SEG license or copyright; see Terms of Use at http://library.seg.org/

reasonable to assume that we might have variations caused by the strength of the source array, the geometry of the source array, and the properties of the sea surface. If the sea surface is very rough, it is fair to assume that the reflected ghost signal will be weaker, and hence there will be fewer cavities created. The sharpness of the main peak of an air-gun source signature depends on the mechanism of the port opening as well as the firing pressure. Therefore, there might be minor differences in the frequency content of the main peak between various manufactures.

For a rough sea surface, the high-frequency signal will be scattered in various directions, and thus the effect of this may be a significant reduction in the reflection coefficient. From underwater acoustics, an approximation for the reflection of sound from a rough water surface is given as (Clay and Medwin, 1977)

$$R = -e^{-2k^2h^2\cos^2\theta}; k = 2\pi f/c, \quad (6)$$

where $h$ is the rms wave height, $f$ is the frequency, $\theta$ is the reflection angle, and $c$ is the sound velocity in water. Equation 6 is valid in the range of $kh \cos\theta < 1$. Figure 15 shows the absolute value of the sea surface reflection coefficient using equation 6 assuming a wave height of 0.5 ms and 1 m. We are probably stretching Clay and Medwin's equation by assuming frequencies as low as 100–500 Hz and wave heights of the order of a meter. However, the figure shows that high frequencies will be attenuated more than lower frequencies, and hence the ghost signal of the main peak of an air-gun signal might be weaker for rougher seas.

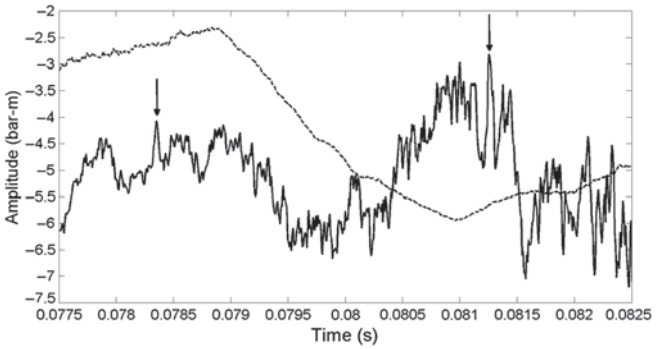



Figure 12. Detail of far-field signatures (shown in Figure 8) measured at the seabed for the 2750 cubic inch source array (solid line) and for the 1430 cubic inch array (dashed line). Notice the significant difference in the high-frequency signal for the big array. Two pronounced spikes (marked by arrows) are observed at 0.0783 and 0.0813 s, respectively.

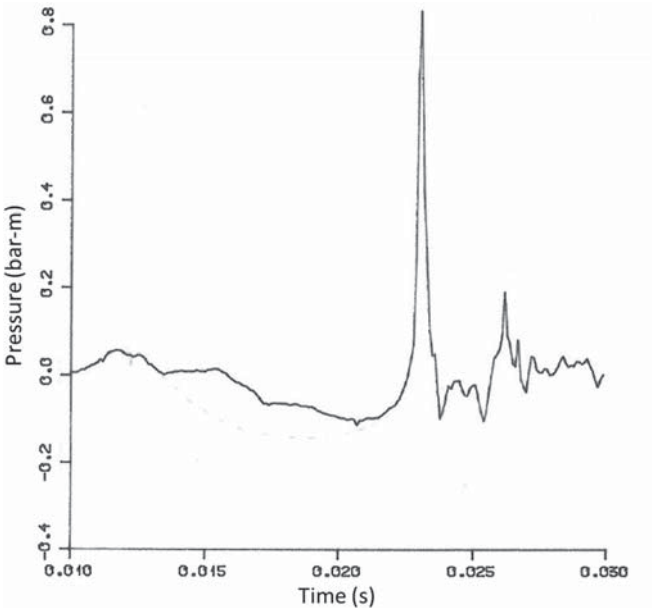



Figure 13. Near-field measurement of a S15 water gun fired at 7.5 m depth. Firing pressure is 100 bar. Measurement made by SERES in 1986. Data acquired using a 800-Hz high-cut filter.

## MODELING THE PRESSURE BETWEEN THE AIR-GUN STRINGS

It might be interesting to model the pressure wavefield in the area where we expect that ghost cavitation might occur. We used a commercial air-gun modeling software based on the theory developed by Ziolkowski (1970). The modeling assumes that the bubble created by the air gun is perfectly spherical and is based on the nonlinear Kirkwood-Bethe equation. It should be noted, however, that the nonlinear effects caused by strong ghost signals are not included in the forward modeling. As the distance between seismic sources reduces, the superposition principle will break down. In particular, if two subarrays are close, it is not necessarily correct to add the ghost signals together. In our modeling, linear superposition is used, and this error might therefore lead to negative absolute pressures in the water, which is of course unphysical. Despite this, we use the linear superposition principle to identify areas (for instance, above one of the subarrays or between them) where the pressure is negative. Our assumption is then that ghost cavitation is likely to occur at these particular locations.

Figure 16 shows the modeled pressure response at 2 m depth above the central streamer for the array configuration shown in Figure 2. We notice that the modeling actually predicts pressure levels that are below an absolute pressure of zero, which is unphysical. This weakness of the source modeling is caused by the fact that nonlinear effects are neglected. As the modeled dynamic pressure at a depth of 2 m is approaching −1.2 bars, nonlinear effects will ensure that pressure levels below zero are not reached. First of all, linear superposition will not be valid, and the sum of all the negative ghost signals will not add up to a big negative number as shown in Figure 16, but a smaller negative value. Furthermore, the phase transition from water to water vapor will start as the absolute pressure approaches zero, and it is indeed this creation of water vapor that is the cause of the high-frequency signals according to our assumption. Despite the fact that we cannot use the linear theory used in the source modeling, it can be used as an indication of possible cavity creation: In Figure 16, the limit for cavity creation is shown by the dashed horizontal line at –1.2 bars. We will assume that cavity creation might occur when the modeled pressure is below this line, which means for modeling times between 8.5 and 11.5 ms. This means that a rough estimate for the start time of cavity creation might be approximately 4–7 ms after the main peak signal of the gun array. From Figure 8, we observe that the traveltime delay between the main peak and the ghost cavitation signal is

Downloaded 10/10/13 to 129.241.27.34. Redistribution subject to SEG license or copyright; see Terms of Use at http://library.seg.org/

approximately 7 ms. When comparing these numbers, we have to add 2 m to the ghost traveltimes (see Figure 9), meaning that the modeled time difference between the peak and ghost signal is approximately 6–9 ms, which is in reasonable agreement with the observed 7 ms. If we assume that the cavities are small, for instance, 1 cm in radius, the collapse time will be approximately 0.8 ms at a 2 m depth (equation 1).

We observe from Figure 16 that if the reflection coefficient of the sea surface is less negative (dashed line), for instance, −0.8 (instead of the ideal value of −1), the ghost signal becomes less negative, and hence, it is likely that less ghost cavitation will occur. We therefore assume that the degree of ghost cavitation depends on the state of the sea surface: For a rough sea surface, there will be less ghost cavitation because the "acoustic mirror" is weaker.

A simpler way to avoid ghost cavitation might be to increase the distance between the subarrays (this was not tried in the experiment described in this paper). Figure 17 shows modeled signatures similar to those in Figure 16, but for a source configuration where the distance between the subarrays is increased from 6 to 10 m. We notice that the ghost signal is significantly reduced in this case. This is an indication that it might be straightforward to attenuate the high-frequency signals created by ghost cavitation. It also means that it might be an indicative experiment to perform: Gradually increase the distance between the subarrays and measure if the amount of high-frequency signals decreases.

## THE WEAK HIGH-FREQUENCY GHOST

Another interesting observation from Figure 8 is that we cannot see a clear ghost signal associated with the high-frequency signal. Depending on the depth where the ghost cavities are formed, we may expect the ghost signal to appear almost instantaneously or delayed by several milliseconds (assuming that they collapse at the same depth as the source corresponds to a delay of 6.6 ms, assuming vertical raypaths). In Figure 18, we identify a weaker signal that is significantly weaker than the high-frequency signal. Whether or not this is the ghost signal is hard to judge. If so, the sea surface reflection coefficient for the high-frequency signal must be significantly less than −1. Figure 19 shows the unfiltered version of shot 20 together with two band-pass-filtered versions: 1–10 and 50–60 kHz. We notice that the amplitude ratio between the potential ghost signal and the maximum peak of the high-frequency signal decreases as frequency increases. There are several potential causes for a lower reflection coefficient with frequency, for instance, the roughness of the sea surface.

Figure 20 shows the absolute value of the reflection coefficient for three rms wave heights: 10, 5, and 1 cm. We clearly see (from equation 2 as well as from Figure 20) that the sea surface reflection coefficient decreases significantly as the frequency of the signal increases. In Figure 20, we have assumed that the reflection angle is 0°.

We think that this surface scatter effect is the major cause for the fact that we do not observe a clear ghost signal for the high-frequency signals produced by an air-gun array. Other causes might be the presence of small air bubbles in the water and shadow effects from equipment located above the air guns. From Figure 7, we notice that the ghost reflection signal seems to be weaker for the shots corresponding to increased incidence angles compared to shot 20, which we assume represents a reflection angle of 0°.

## COMPARISON WITH MARINE MAMMAL EXPOSURE CRITERIA

One of the first attempts to define scientific criteria to quantify the magnitude and frequency properties of marine noise that might change marine mammal behavior was the work published by Southall et al. (2007). In that paper they introduce three so-called *M*-weighting functions: the low-, mid-, and high-frequency cetacean functions. The *M*-function is meant as a guide to focus on the frequency band that is most critical for marine mammals. However, it is stated by Southall et al. (2007) that "the functions are quite precautionary, which is appropriate given that data are limited or lacking for most species".

Figure 21 shows a comparison between the three *M*-functions and the frequency spectrum estimated from the seabed hydrophone recording (approximately 55 m away from the source) for the full array (black solid line), one subarray (blue solid line), and a single

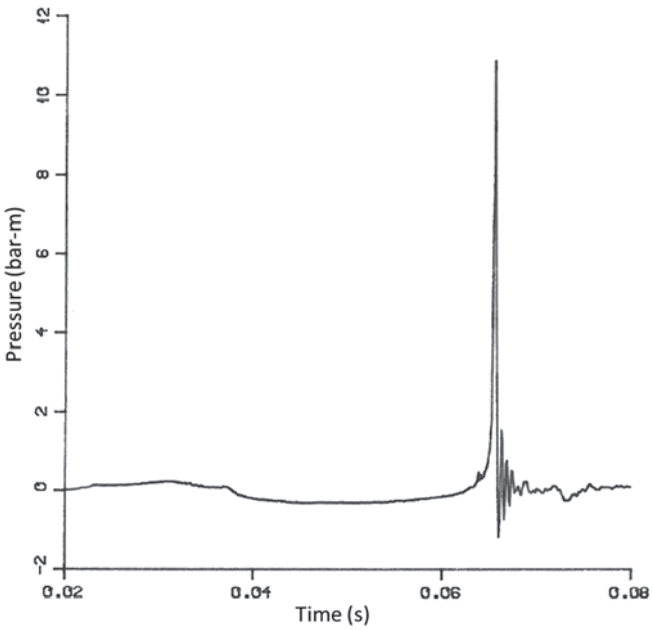



Figure 14. Near-field measurement of a P400 water gun fired at 7.5 m depth. Firing pressure is 100 bar. Measurement made by SERES in 1986. Data acquired using a 800-Hz high-cut filter.

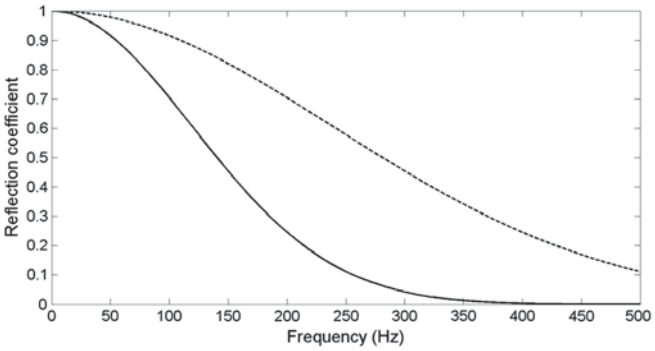



Figure 15. Absolute value of the sea surface reflection coefficient assuming wave heights of 0.5 (dashed line) and 1 m (solid line).

Downloaded 10/10/13 to 129.241.27.34. Redistribution subject to SEG license or copyright; see Terms of Use at http://library.seg.org/

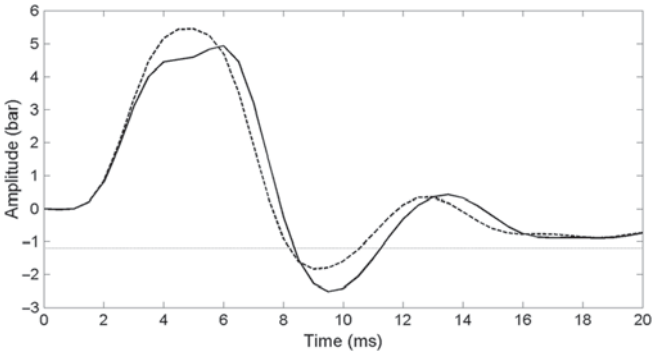



Figure 16. Modeled dynamic pressure signal assuming sea surface reflection coefficients of −1 (solid line) and −0.8 (dashed line) at 2 m depth, located at the center of the three-string gun array (Figure 2). The dotted line indicates the level for zero absolute pressure (equal to the negative value of the hydrostatic pressure). If we assume that cavities are formed when the absolute pressure is lower than zero, it will occur between 8 and 11 ms for both cases.

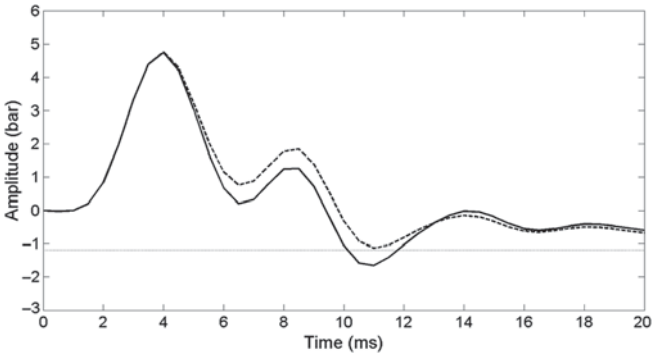



Figure 17. The effect of increasing the distance between the air-gun subarrays: Modeled dynamic pressure signal assuming sea surface reflection coefficients of −1 (solid line) and −0.8 (dashed line) at 2 m depth, located at the center of the three-string gun array (Figure 2) when the distance between the subarrays is increased from 6 to 10 m. The dotted line indicates the level for zero absolute pressure (equal to the negative value of the hydrostatic pressure). If we assume that cavities are formed when the absolute pressure is lower than zero, it will occur between 8 and 11 ms for both cases.

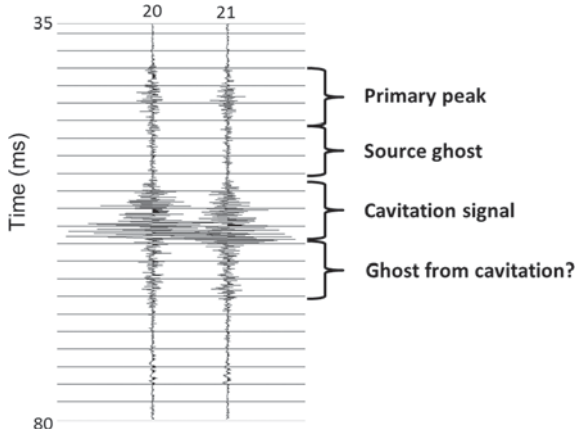



Figure 18. High-pass-filtered (10–62.5 kHz) versions of shots 20 and 21 showing potential ghost signal of the high-frequency signal delayed by 6–7 ms.

gun (red solid line). The full array response has been normalized to zero for the max peak of the spectrum. Furthermore, a smoother has been applied to the data prior to normalizing. The same scalar has been applied to the three far-field measurements, so that it should be possible to compare the full array, one string, and a single gun in this figure. We clearly observe that all three sources emit significant energy within the lower part of the low-frequency cetacean M-function. For the mid- and high-frequency *M*-functions, we observe that the measured far-field signals decays as the *M*-functions increase (for frequencies between 100 and 1000 Hz).

Because the experimental data and the *M*-function curves are scaled differently, it is hard to quantify for instance whether a signal of –60 dB for frequencies around 10 kHz is significant or not.

## DISCUSSION

It is important to underline that the mechanism for the high-frequency signals (10–20 kHz) observed in the data analyzed in this paper is still not clear to us. From water-gun signatures, we have estimated the initial cavity radius ranging from 4 to 20 cm from the smallest water gun (S15) to the largest (P400). The signals recorded

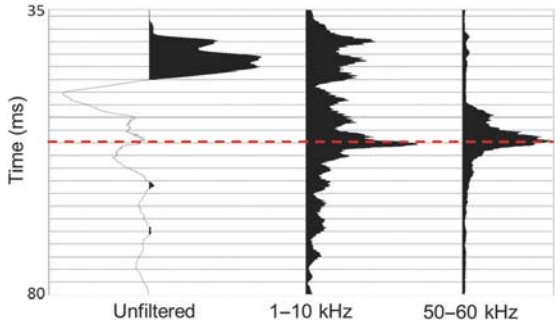



Figure 19. Comparison of unfiltered trace (left), 1–10 kHz band-pass-filtered trace (middle, after multiplication with 50), and 50–60 kHz (right, after multiplication with 400). The two right traces have been smoothed using a 1 ms window after taking the absolute value of the samples. The high-frequency noise appears with a maximum around 56 ms (marked by the dashed line). There is 2 m between each time line on this plot. For the 1–10 kHz data, we observe several events that could be interpreted as ghost signals, while similar events are weaker for the 50–60-kHz data.

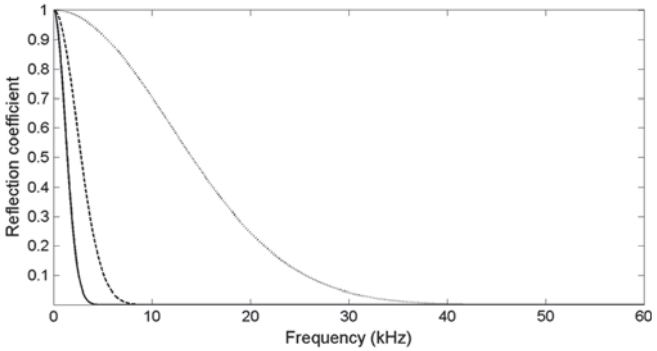



Figure 20. Modeled sea surface reflection coefficient (absolute value) assuming an rms wave height of 10 (solid line), 5 (dashed line), and 1 cm (dotted line).

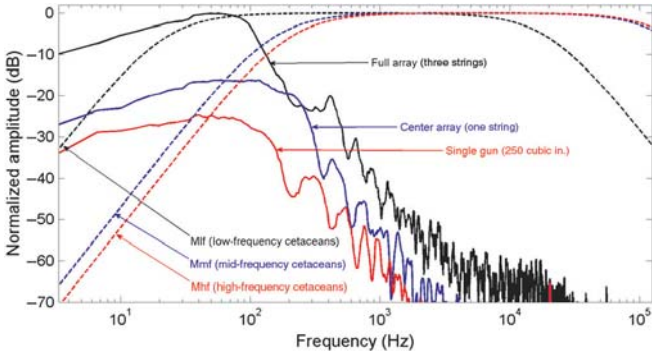



Figure 21. Comparing the far-field hydrophone data with M-weighting functions for low-, mid-, and high-frequency cetaceans. The full array data have been normalized to zero, and the same normalizing factor has been used for the center array data and the single gun data.

from these water guns are very different from the high-frequency signals we observe in this data set. A collapse caused by a water-gun cavity of 4 cm gives rise to a collapse signal that is clearly observable for frequencies below 1 kHz, while our high-frequency signals are observable only for frequencies above 5–10 kHz. Furthermore, we observe a plurality of collapse signals, indicating that the number of cavities is large.

Some of this plurality might be explained by the plurality in the acquisition setup: The ghost signals from each gun in the array will reach a specific location at different times causing a fairly complex pressure field in the water surrounding the air-gun array.

Maybe the roughness of the sea surface might contribute to a heterogeneous pressure distribution in the water between the air-gun strings? Only carefully designed experiments can help us to find out more about this.

In Landrø et al. (2011), a strong peak around 20 kHz is observed for the ambient noise data (blue and green lines) in Figure 17. We do not know the cause of this high-frequency noise, but it is clear that it is not caused by ghost cavitation or other effects connected to the air guns. Because this noise is almost at the same level as the full array data (red line in Figure 17), one should be careful to draw any conclusions for this particular frequency.

## CONCLUSIONS

We find that the high-frequency signal in the 10–20 kHz range generated by a conventional marine air-gun array is repeatable from shot to shot. Our analysis shows that it is not repeatable with respect to minor details; however, what we observe is that the envelope of these high-frequency signals is highly repeatable. The main peak of the high-frequency signal occurs approximately 7–14 ms after the main peak of the source signature. The ghost signal of the high-frequency signal is not observed in our data, and this is attributed to scattering effects caused by a nonsmooth sea surface.

## ACKNOWLEDGMENTS

ML wants to thank the Norwegian Research Council for financial support to the ROSE Consortium at NTNU. We want to thank E. Nielsen and G. Zaalberg-Metselaar for acquiring the near-field source signatures of water guns used in this paper. The paper has benefited significantly from constructive comments and suggestions given by the reviewers, J.-F. Hopperstad, T. Elboth, and one anonymous reviewer.

## REFERENCES

Amundsen, A., and M. Landrø, 2010, Marine seismic sources, Part V: The hearing of marine mammals: GeoExpro, **7**, no. 6, 64–66.
Amundsen, A., and M. Landrø, 2011a, Marine seismic sources, Part VI: High frequency signals from air guns: GeoExpro, **8**, no. 1, 69–71.
Amundsen, A., and M. Landrø, 2011b, Marine seismic sources, Part VII: Fish are big talkers: GeoExpro, **8**, no. 2, 64–67.
Breitzke, M., O. Boebel, S. El Naggar, W. Jokat, and B. Werner, 2008, Broad-band calibration of marine seismic sources used by R/V Polarstern for academic research in polar regions: Geophysical Journal International, **174**, 505–524, doi: 10.1111/j.1365-246X.2008.03831.x.
Clay, C. S., and H. Medwin, 1977, Acoustical oceanography: Principles and applications: John Wiley & Sons.
Goold, J. C., and P. J. Fish, 1998, Broadband spectra of seismic survey air-gun emissions, with reference to dolphin auditory thresholds: Journal of the Acoustical Society of America, **103**, 2177–2184, doi: 10.1121/1.421363.
Groenaas, H. S. G., S. A. Frivik, A. S. Melboe, and M. Svendsen, 2011, A novel marine mammal monitoring system utilizing the seismic streamer spread: 73rd Annual International Meeting, EAGE, Extended Abstracts, D047.
Harrison, M., 1952, An experimental study of single bubble cavitation noise: Journal of the Acoustical Society of America, **24**, 776–782, doi: 10.1121/1.1906978.
Landrø, M., L. Amundsen, and D. Barker, 2011, High-frequency signals from air-gun arrays: Geophysics, **76**, no. 4, Q19–Q27, doi: 10.1190/1.3590215.
Landrø, M., G. Zaalberg-Metselaar, B. Owren, and S. Vaage, 1993, Modeling of water-gun signatures: Geophysics, **58**, 101–109, doi: 10.1190/1.1443339.
Laws, R. M., 2010, Cetacean hearing-damage zones around a seismic source, *in* A. N. Popper, and A. Hawkins, eds., The effects of noise on aquatic life: Springer Science+Business Media, LLC, Advances in Experimental Medicine and Biology, 473–476.
Plesset, M. S., and A. T. Ellis, 1955, On the mechanism of cavitation damage: Transactions of the ASME, **77**, 1055–1064.
Rayleigh, O. M., 1917, On the pressure developed in a liquid during the collapse of a spherical cavity: Philosophical Magazine, **34**, no. 200, 94–98, doi: 10.1080/14786440808635681.
Southall, B. L., A. E. Bowles, W. T. Ellison, J. J. Finneran, R. L. Gentry, C. R. Greene, Jr., D. Kastak, D. R. Ketten, J. H. Miller, P. E. Nachtigall, W. J. Richardson, J. A. Thomas, and L. Tyack, 2007, Marine mammal noise exposure criteria: Initial scientific recommendations: Aquatic Mammals, **33**, no. 4, 411–521, doi: 10.1578/AM.33.4.2007.411.
Ziolkowski, A., 1970, A method for calculating the output pressure waveform from an air gun: Geophysical Journal of the Royal Astronomical Society, **21**, 137–161, doi: 10.1111/j.1365-246X.1970.tb01773.x.

Downloaded 10/10/13 to 129.241.27.34. Redistribution subject to SEG license or copyright; see Terms of Use at http://library.seg.org/